Effect of Temperature on Ionic Conductivity and Optical Bandgap Features of TSP-NaI-Based Biopolymer Electrolytes

M. Keerthi[1], M. Gnana Kiran[1,*], Prakash Babu Kanakavalli[2], Vinjamuri Venkata Kamesh[3], R. L. Krupakaran[4], P. S. V. Nandini[1], N. Krishna Jyothi[5], M. C. Rao[6], D. Madhavi Latha[7], SK. Mahamuda[1]

* *gnanakiran33@gmail.com*

[1] Department of Physics, Koneru Lakshmaiah Education Foundation, Vaddeswaram-522302, AP, India
[2] Department of Mechanical Engineering, Velagapudi Ramakrishna Siddhartha Engineering College, Deemed to be University, Vijayawada-520007, A.P, India
[3] Department of Mechanical Engineering, Aditya University, Surampalem-533437, EG Dt, A.P, India
[4] Department of Mechanical Engineering, Mohan Babu University, Sree Vidyanikethan, Tirupati-517102, AP, India
[5] Department of Physics, Sri Sathya Sai University for Human Excellence, Kalaburagi, Karnataka, India
[6] Department of Physics, Andhra Loyola College, Vijayawada-520008, India
[7] Department of Physical Sciences, Kakatiya Institute of Technology and Science, Warangal -506 015, Telangana, India

Abstract: This research systematically examines the structural, electrical, and optical characteristics of Tamarind Seed Polysaccharide (TSP)-based biopolymer electrolytes doped with varying concentrations of sodium iodide (NaI). Composite films were synthesised using the solution-cast technique in weight-per cent ratios of TSP:NaI (100:0, 90:10, 80:20, and 70:30) and subsequently characterised using X-ray diffraction (XRD), Fourier-transform infrared spectroscopy (FTIR), UV–Vis spectroscopy, and impedance analysis. The XRD analysis indicated that the 80:20 composition displayed the highest degree of amorphousness, which is associated with improved ionic conductivity and reduced crystallite size. The FTIR analysis corroborated the formation of a complex between TSP and NaI, while the temperature-dependent conductivity measurements exhibited Arrhenius behaviour, with the 80:20 film exhibiting the highest ionic conductivity (1.97×10^{-4} S/cm) and the lowest activation energy (0.69 eV). Optical absorption investigations revealed a decrease in the bandgap from 3.92 (pure TSP) to 2.68 eV (80:20 film). Minimum optical energy band gaps were achieved for the optimised film. Opto-dielectric investigations further demonstrated that the 80:20 formulation exhibited optimal dielectric permittivity and loss. The results underscore the potential applicability of TSP–NaI biopolymer systems as sustainable, high-performance polymer electrolytes.

Keywords: TSP, Sodium iodide (NaI), Arrhenius relation, Tangent loss, Optical dielectric loss.

1. INTRODUCTION

Polymer electrolytes are of paramount significance in electrochemical cells and membrane technology. Cells function as ion-conducting membranes, thereby facilitating ionic transport, which is crucial for energy production. The unique attributes of polymer electrolytes, including their inherent flexibility, non-flammability, and superior interfacial contact with electrodes, are driving their integration into an increasingly diverse array of applications, particularly in electrochemical devices. A particularly notable application of polymer electrolytes resides in batteries, with a focus on lithium-ion batteries (LIBs) and the emerging class of lithium-metal batteries [1]. Moreover, polymer electrolytes are employed in a range of advanced electrochemical devices, including batteries, rechargeable batteries, supercapacitors, and electrochromic devices. Their capacity to facilitate ionic conduction while preserving mechanical flexibility renders them exceptionally well-suited for these applications, thereby enabling the development of flexible and solid-state devices. They provide substantial safety enhancements by substituting solid electrolytes, thereby reducing the hazards associated with fire, explosion, and leakage. Polymer electrolytes are instrumental in augmenting energy density, prolonging cycle life, and enhancing dendrite suppression in these battery systems. Additionally, they are being investigated for utilization in alternative battery chemistries.

Polymer electrolytes can be extensively categorised into various classifications based on their composition and physical state, each offering unique benefits for a multitude of electrochemical applications. Solid Polymer Electrolytes (SPEs), commonly referred to as dry polymer electrolytes, generally

represent solvent-free configurations in which an inorganic salt is dissolved directly within a polymeric matrix. The mobility of ions within SPEs is intimately associated with the segmental dynamics of the polymer chains, rendering their ionic conductivity highly sensitive to temperature variations. Although they provide exceptional safety profiles, their comparatively low ionic conductivity at ambient temperature constrains certain applications. In contrast, Gel Polymer Electrolytes (GPEs) incorporate a liquid plasticiser (frequently an organic solvent or ionic liquid) into the polymeric matrix [2]. This liquid phase markedly enhances ionic conductivity by providing a medium that facilitates accelerated ion diffusion, effectively bridging the characteristics of liquid and solid electrolytes. Nonetheless, GPEs may still encounter challenges related to solvent leakage and flammability, albeit to a lesser extent than entirely liquid electrolytes. Ultimately, Composite Polymer Electrolytes (CPEs) amalgamate inorganic fillers within a polymer matrix. These filters can fulfil several functions: they can augment mechanical strength and diminish polymer crystallinity to boost ionic conductivity. CPEs aspire to harmonise the benefits of both solid and liquid electrolytes, delivering a judicious equilibrium of elevated ionic conductivity, mechanical resilience, and enhanced safety.

The synthesis of biopolymer electrolytes generally entails methods that promote the dissolution and thorough incorporation of the biopolymer host with an ionic conductive salt. The most prevalent and straightforward methodology employed is the solution cast technique. Within this framework, the biopolymers (for instance, starch, cellulose derivatives, and chitosan, pectin, agar, and tamarind seed polysaccharides) are initially solubilised in an appropriate solvent (typically water or dilute acid, contingent upon the solubility of the biopolymer) [3]. Subsequently, the requisite ionic salt (for example, lithium salts such as $LiClO_4$, $LiCF_3SO_3$ or ammonium salts like NH_4SCN, as well as sodium salts such as $NaNO_3$ and NaI) is incorporated into the biopolymer solution, thoroughly stirred to ensure a homogeneous mixture and complexation between the polymer and the salt. The resultant homogeneous solution is then deposited onto a flat substrate (such as a Petri dish) and allowed to dry gradually at ambient or slightly elevated temperatures. Throughout the drying phase, the solvent evaporates, culminating in a flexible, self-supporting biopolymer electrolyte film.

Tamarind Seed Polysaccharide (TSP), a naturally occurring and environmentally sustainable bio-polymer, is recognised for its remarkable film-forming capabilities, extensive pH adaptability, and biocompatibility [4]. It features a distinctive branched architecture composed of a β-(1,4)-D-glucan backbone interspersed with α-(1,6)-D-xylose branches, which are partially substituted with β-(1,2)-D-galactose. These attributes enhance its efficacy as a polymer host, offering a stable yet flexible matrix conducive to ion transport. The intrinsic gelling and thickening characteristics of TSP further facilitate the formation of self-standing electrolyte membranes.

Sodium Iodide (NaI) serves as the ionic dopant, supplying mobile Na^+ ions that are critical for conduction. As an ionic salt, NaI readily dissociates in an appropriate polymer matrix, liberating highly mobile Na^+ cations and I^- anions. NaI imparts several significant properties to the polymer electrolyte. Its high solubility in numerous polar solvents, typically employed in the synthesis of polymer electrolytes, ensures homogeneous dispersion and effective complexation with the polymer host. This elevated solubility also increases the concentration of free ions, which is directly correlated with conductivity. The presence of NaI may also affect the morphology and crystallinity of the polymer matrix [5]. Lastly, NaI exhibits relative stability under standard operating conditions for various electrochemical devices, although precautions are often taken during storage to prevent oxidation by atmospheric oxygen, which can induce yellow discolouration due to the formation of triiodide complexes.

The combination of TSP with $LiClO_4$ can yield solid polymer electrolytes exhibiting favourable ionic conductivity of 8.77×10^{-4} Scm^{-1} at ambient temperature [6]. An investigation focused on TSP with $NaNO_3$ indicated a maximum ionic conductivity of 1.14×10^{-4} Scm^{-1} for a specific optimised formulation [7]. A significant study revealed a maximum ionic conductivity of 1.97×10^{-3} Scm^{-1} for a TSP/$Mg(NO_3)_2$ formulation at room temperature [8]. The combination of TSP with NH_4SCN can yield an ionic conductivity of 2.85×10^{-4} Scm^{-1} at ambient temperature [9]. These instances exemplify the versatility of Tamarind Seed Polysaccharide as a biopolymer host and its ability to form solid polymer electrolytes with various ionic salts, yielding a range of ionic

conductivities suitable for diverse electrochemical device applications. The amalgamation of Tamarind Seed Polysaccharide (TSP) with Sodium Iodide (NaI) represents an intriguing and increasingly pertinent domain of inquiry in the advancement of solid polymer electrolytes, particularly for battery applications, owing to several notable aspects of its innovation. While TSP has been investigated in conjunction with various salts, the specific advantages conferred by NaI, especially within the context of emerging sodium-ion battery technology, underscore its significance. This investigation articulates an innovative methodology by formulating biopolymer electrolytes derived from Tamarind Seed Polysaccharide (TSP) and Sodium Iodide (NaI), a synergistic combination that has not been previously optimised for solid-state applications. Prospective research endeavours may focus on enhancing the electrochemical stability and long-term durability of TSP-NaI biopolymer electrolytes under realistic device operating conditions. Furthermore, incorporating this electrolyte system into sodium-ion battery prototypes would facilitate evaluation of its performance in practical scenarios and its potential commercial applicability.

2. EXPERIMENTAL PROCEDURES

2.1. Synthesis of the Material

'Tamarind seed polysaccharide (TSP)' was acquired from 'TCI Chemicals, whereas 'Sodium Iodide' (NaI) was sourced from 'Merck'. The films were synthesised using the solution-casting technique, employing 30 ml of double-distilled water (H_2O) as the solvent and various weight-percentage ratios of TSP:NaI (100:00, 90:10, 80:20, 70:30), and were stirred for 12 h at 60°C. The resultant homogeneous solution was transferred into Petri dishes and subsequently maintained at 60°C within a vacuum chamber for 24 h. The resultant biopolymer electrolyte film was meticulously extracted from the dishes and subsequently placed into a vacuum desiccator for further investigations.

2.2. Characterization

The 'X-ray diffraction (XRD)' patterns of the synthesised biopolymeric membranes were obtained utilising an 'XPERT-PRO diffractometer' across 2θ angles ranging from 10° to 80°, employing 'Cu Kα radiation' at a voltage of 40 kV and a current of 30 mA. FTIR spectra were recorded at 303 K using a SHIMADZU-8000 FTIR Spectrophotometer in the wave number range 400–4000 cm^{-1} with a resolution of 4 cm^{-1}.

The 'impedance' measurements were conducted employing blocking stainless steel electrodes within the frequency range of 42 Hz to 1 MHz, facilitated by the 'HIOKI 3532–50 LCR' meter. 'Ultraviolet-visible (UV–Vis) spectroscopy' analysis was executed at ambient temperature utilizing the 'JASCO V-670 UV–VIS–NIR' spectrophotometer.

3. RESULTS AND DISCUSSION

3.1. Analysis of Crystallinity by XRD Technique

XRD is a traditional technique used to elucidate the crystalline architecture and phase composition of a given material. The accompanying XRD patterns (Fig. 1) and the associated tabulated data provide valuable insights into the structural modifications of TSP upon the incorporation of varying concentrations of NaI. The principal aim of this investigation is to elucidate the influence of NaI integration on the crystallinity of the composite material. The XRD analysis shows the diffraction profiles of the pure TSP biopolymer compared with the TSP biopolymer at different NaI concentrations. The pure TSP (100:0) exhibits a broad diffraction peak centred approximately at 2θ= 19.8°, suggesting an amorphous or poorly crystalline configuration. With the incremental addition of NaI, a notable reduction in the intensity of the crystalline peak of the salt-doped TSP biopolymer electrolyte films was observed. The most diminished intensity peak, observed for TSP:NaI (80:20 wt.%), corroborated the highest amorphous nature and the minimised crystalline dimensions. A few small, sharp diffraction peaks were noted in the 30% film, indicating that the salt was not entirely dissolved within the biopolymer matrix. This phenomenon can be comprehensively understood by computing crystallite sizes from the XRD peaks, utilising the Scherrer equation provided in [10].

$$D= \frac{K\lambda}{\beta \cos \theta} \tag{1}$$

Where 'D represents the crystallite size, 'θ denotes the Bragg angle, 'λ signifies the wavelength, 'β corresponds to the full width at half maximum (FWHM)' value, and 'K represents the Scherrer constant (0.9)'. The particle size measurements were ascertained employing the Scherrer equation for the 'TSP:NaI' films, which are detailed in Table 1. Based on the computations of crystallite size, it

was concluded that the biopolymer film 'TSP:NaI' (80:20 wt.%) exhibited a minimal crystallinity value of 0.31 nm, indicating a predominant degree of amorphousness in comparison to other compositions.
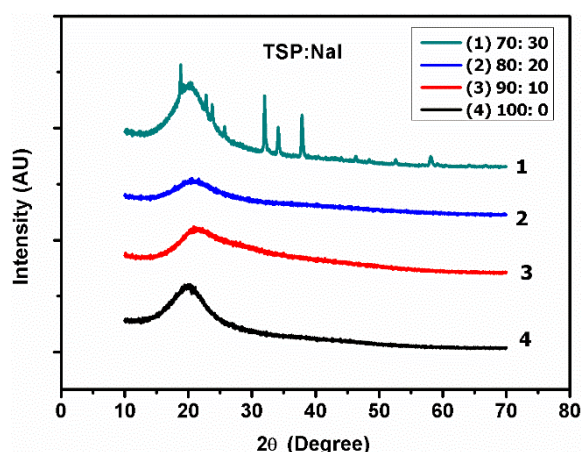

Fig. 1. Crystalline comparison of TSP:NaI compositions at various wt.% ratios

Table 1. Crystallography dimensions of TSP:NaI at varying weight percentage ratios

Composition of TSP:NaI	2θ	$\cos\theta$	FWHM (rad)	D (nm)
100:0	19.8	0.98	0.2464	0.57
90:10	20.9	0.983	0.3775	0.39
80:20	20.4	0.98	0.3785	0.31
70:30	20.4	0.98	0.2181	0.55

3.2. Analysis of Bond Interactions by Fourier Transform Infrared Spectroscopy (FTIR)

A proficient approach to elucidating localised structural modifications in polymers is Fourier Transform Infrared Spectroscopy (FTIR). The analysis of vibrational frequencies facilitates the identification of bonding types and various functional groups inherent within the polymer matrix [11]. The FTIR spectra for the unadulterated 'TSP' are depicted in Fig. 2(a), alongside the spectra for films comprising various weight percentage ratios of NaI (Fig. 2(b-d)) within the wave number spectrum of 450–4000 cm^{-1}, with corresponding assignments detailed in Table 2. The prominent peak observed at 3325 cm^{-1} for pure 'TSP' is attributed to the stretching of a hydroxyl group (N-H). The additional peaks identified at wave numbers 3313 cm^{-1}, 3332 cm^{-1}, and 3307 cm^{-1} correspond to the weight percentage ratios of 90:10, 80:20, and 70:30, respectively. This observed variation may indicate interactions between the hydroxyl groups of the host polymer and the cations from the incorporated salt. The C-H stretching has resulted in an absorption peak at 2894 cm^{-1}, which has subsequently shifted to 2875 cm^{-1} in the 90:10 ratios, 2882 cm^{-1} in the 80:20 ratios, and 2888 cm^{-1} in the 70:30 ratios of the samples, respectively. With the incremental addition of salt, novel peaks in the salt-modified system at 2368 cm^{-1}, 2355 cm^{-1}, and 2348 cm^{-1} for the 90:10, 80:20, and 70:30 films have emerged, which are attributed to O=O=O stretching, thereby demonstrating the interaction between the host polymer 'TSP' and the doping salt NaI.

The N-H bending observed in pure 'TSP' at 1645 cm^{-1} has been observed to shift to a lower wavenumber in all electrolytes containing salt-incorporated polymers. An absorption peak resulting from O-H bending at 1340 cm^{-1} has shifted to 1359 cm^{-1} in the 90:10 ratios, 1365 cm^{-1} in the 80:20 ratios, and 1353 cm^{-1} in the 70:30 ratios of the samples, respectively. A peak associated with pure 'TSP' is located at 1016 cm^{-1}. The supplementary peaks at 1022 cm^{-1}, 1004 cm^{-1}, and 1009 cm^{-1} correspond to the weight percentage ratios of 90:10, 80:20, and 70:30, respectively, and are ascribed to C=O stretching, which also demonstrates a minimal number of transitions across the TSP:NaI matrix. In addition to variations among these distinct peaks, alterations in peak intensities and widths have also been observed, corroborating the formation of a complex between TSP and NaI.

Table 2. Spectral band designations for different weight percent ratios of TSP:NaI

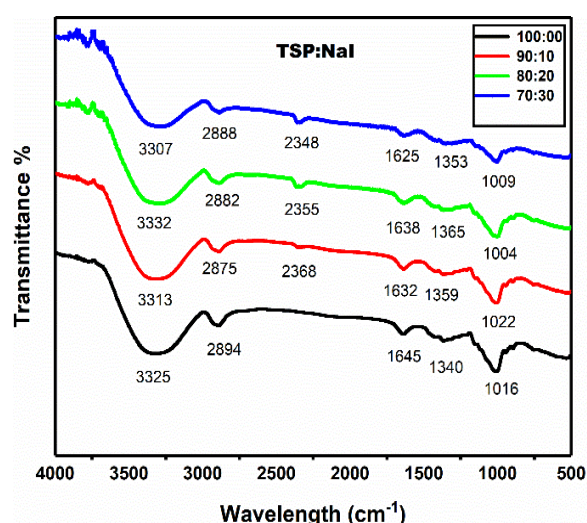| Wave number (cm^{-1})				Assignment
70:30	80:20	90:10	100:0	
3307	3332	3313	3325	N-H stretching
2888	2882	2875	2894	C-H stretching
2348	2355	2368		O=O=O stretching
1625	1638	1632	1645	N-H bending
1353	1365	1359	1340	O-H bending
1009	1004	1022	1016	C=O stretching

Fig. 2. FTIR spectra of a) pure TSP, b) 90:10, c) 80:20, d) 70:30 wt.% ratios of TSP-NaI

3.3. Analysis of the Temperature Dependency of Electrical Conductivity

The presented graphical representation examines the temperature-dependent ionic conductivity of a composite electrolyte system comprising '80% TSP and 20% NaI'. The data are shown as a logarithmic plot of ionic conductivity (log σ) against the inverse temperature (1000/T), which is a typical Arrhenius-type analysis frequently employed to determine the activation energy in ionic conductors [12]. The linear Arrhenius behaviour suggests that ionic transport likely transpires through a hopping mechanism facilitated by thermal activation. The temperature-dependent ionic conductivity of the synthesised biopolymer membranes is depicted in Fig. 3. The figure indicates that the regression values of the plot are approximately unity, thereby affirming that the biopolymer membranes exhibit Arrhenius behaviour. As the temperature elevates, the movement of ions from one site to adjacent sites intensifies, resulting in improved conductivity. A linear decline in 'log σ' with an increase in '1000/T' corroborates Arrhenius behaviour. The linearity of the data substantiates the following Arrhenius equation:

$$\sigma = \sigma_0 \exp(-\frac{E_a}{KT}) \qquad (2)$$

Taking logarithms on both sides:

$$\log \sigma = (\log \sigma_0) - (\frac{E_a}{2.303kT}) \qquad (3)$$

Here, the slope of the line corresponds to $-(\frac{E_a}{2.303kT})$ allowing the calculation of the activation energy (E_a) pertinent to ion transport. Where 'σ_0' signifies the pre-exponential factor, 'k' denotes

the Boltzmann constant, and 'T' represents the temperature. The figure shows that the membrane exhibiting the highest conductivity (80% TSP: 20% NaI) has a lower activation energy for ionic migration. The linear Arrhenius behaviour can be attributed to the film's predominant amorphous characteristics. The minimum activation energy was determined to be 0.69 eV for the most conductive (80:20) film; such low activation energies are favourable for practical applications. The 80:20 composition indicates an optimal equilibrium in which an adequate amount of Na^+ is present for conduction while the matrix concurrently preserves its structural integrity. Materials of this nature are of considerable interest in the domain of solid-state batteries. The incorporation of economical, readily available salts such as 'NaI' and the polymer 'TSP' may significantly aid in the advancement of sustainable and scalable energy materials.
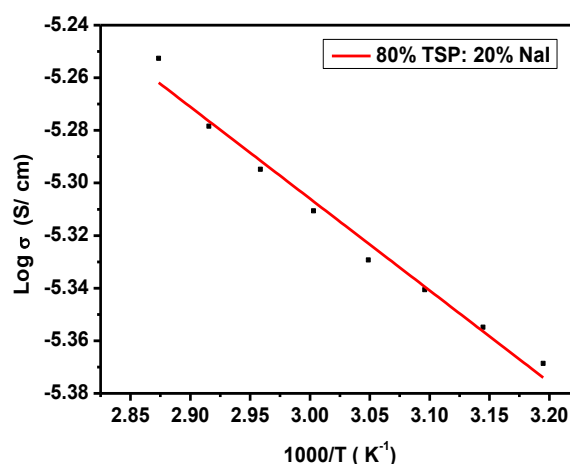

Fig. 3. Arrhenius behaviour plot for TSP-NaI at various wt.% ratios

3.4. Behaviour of Dielectric Permittivity

The graphical representation (Fig. 4) delineates the fluctuations of the fundamental component of dielectric permittivity (ε^1) as a function of frequency for three distinct formulations of TSP:NaI composites, specifically, 90% TSP:10% NaI, 80% TSP:20% NaI, and 70% TSP:30% NaI. This investigation seeks to ascertain the extent to which varying concentrations of NaI impact the dielectric response of the material system across a frequency spectrum ranging from 1 Hz to 1 MHz. At lower frequencies, all formulations exhibit markedly elevated dielectric permittivity, with the 80% TSP:20% NaI specimen exhibiting the most

123

significant response, reaching 5.31×10^4. This notable escalation is predominantly attributed to electrode and interfacial polarisation. The accumulation of space charges at grain boundaries or phase interfaces is a contributing factor to this heightened ε^1. The augmented response observed in the 80:20 formulation indicates that this composition achieves an optimal equilibrium between the insulating TSP matrix and the conductive NaI component. As the frequency escalates, ε^1 experiences a rapid decline before ultimately stabilising for all three formulations. This phenomenon is characteristic of dielectric materials and arises from the inability of dipolar or interfacial polarisation mechanisms to synchronise with the alternating electric field at elevated frequencies [13]. The attenuation of ε^1 at higher frequencies signifies diminished interfacial polarisation.
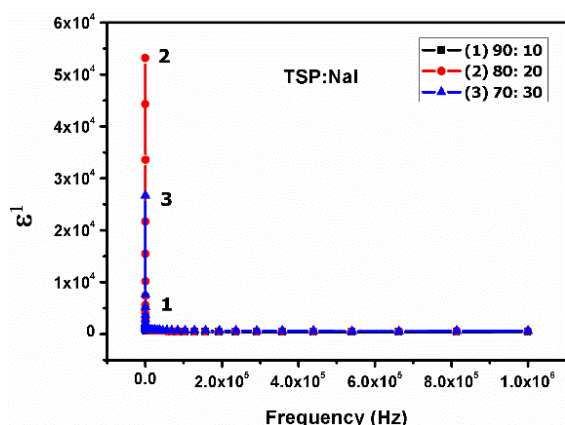

Fig. 4. Dielectric Permittivity plot for TSP-NaI at different wt.% ratios

Among all formulations, the 80% TSP:20% NaI composition demonstrates the highest dielectric permittivity, as outlined in Table 3. The diminished response observed in the 10% NaI formulation is likely attributable to an inadequate concentration of mobile Na$^+$ ions, resulting in reduced polarisation. Conversely, the 30% NaI formulation may experience ion aggregation or saturation.

The 80:20 composition likely achieves optimal ion mobility and dispersion, facilitating maximal space-charge accumulation and polarisation. The frequency-dependent dielectric analysis substantiates that NaI concentration critically modulates the dielectric behaviour of TSP-based composites. The 80% TSP:20% NaI formulation emerges as the most efficacious dielectric material among the evaluated compositions due to its superior polarisation capabilities at lower frequencies.

3.5. Behaviour of Dielectric Loss

The presented Fig. 5 delineates the fluctuation of the imaginary component of the dielectric permittivity (ε^{11}), frequently referred to as dielectric loss, in relation to frequency for TSP:NaI composites characterised by three distinct compositions: 90% TSP:10% NaI, 80% TSP:20% NaI, and 70% TSP:30% NaI. Here, the dielectric properties of pure 'TSP' were taken from the literature [3]. This investigation seeks to elucidate the impact of varying NaI concentrations on energy dissipation within the material across an extensive frequency spectrum. Dielectric loss serves as an indicator of the material's inefficiency in storing electrical energy, which is conventionally linked to conduction phenomena and the relaxation processes of polarisation.
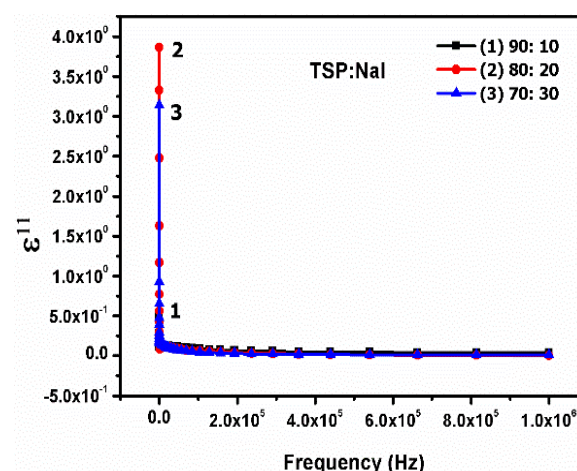

Fig. 5. Dielectric dissipation (Loss) plot for TSP-NaI at different wt.% ratios

At lower frequencies, the dielectric loss is markedly elevated across all compositions, with a notable peak in the 80% TSP:20% NaI specimen, which reaches approximately 3.82 (Table 3). This pronounced loss is ascribed to interfacial polarisation alongside the long-range migration of charge carriers. In heterogeneous systems such as these composites, the accumulation of charges at grain boundaries and the interfaces between the TSP and NaI phases results in substantial energy loss under the influence of a slowly fluctuating electric field. The predominance of dielectric loss in the 80:20 composition implies heightened ionic mobility and the presence of space charge effects, which augment conduction-related losses.

Table 3. Dielectric parameters of TSP-NaI at different wt.% ratios

S. No	Composition of TSP:NaI	ε^1	ε^{11}	Tan δ	Reference
1	100: 0	0.38×10^4	0.36	2.45×10^{-4}	[3]
2	90:10	0.45×10^4	0.49	2.26×10^{-4}	
3	80:20	5.31×10^4	3.82	2.12×10^{-4}	
4	70:30	2.72×10^4	3.23	1.81×10^{-4}	

With increasing frequency, ε^{11} for all compositions exhibits a steep decline, followed by stabilisation, approaching values near zero. At elevated frequencies, the mobile ions and dipolar entities are unable to synchronise with the rapid fluctuations of the electric field, diminishing their role in polarisation and, subsequently, in dielectric loss [13]. This reduction signifies that energy dissipation becomes negligible at higher frequencies, with the dielectric behaviour being predominantly governed by intrinsic material properties, such as electronic polarisation, which contribute minimally to energy loss. Among the three compositions examined, the 80% TSP:20% NaI specimen consistently exhibits the highest level of dielectric loss. The relatively lower loss observed in the 10% NaI specimen indicates diminished ion mobility attributable to inadequate salt concentration. Conversely, while the presence of 30% NaI provides an enhanced source of ions, an excessive salt concentration may lead to ion aggregation or saturation, thereby constraining further increases in polarisation-associated loss. The 20% NaI composition appears to strike an optimal equilibrium, facilitating maximum ionic movement and interfacial effects, albeit at the expense of heightened dielectric loss. The frequency-dependent behaviour of dielectric loss in TSP–NaI composites unveils critical insights into their conduction and polarisation mechanisms. The 80% TSP:20% NaI composition reveals the highest dielectric loss at lower frequencies, signifying robust interfacial polarisation and enhanced ionic mobility.
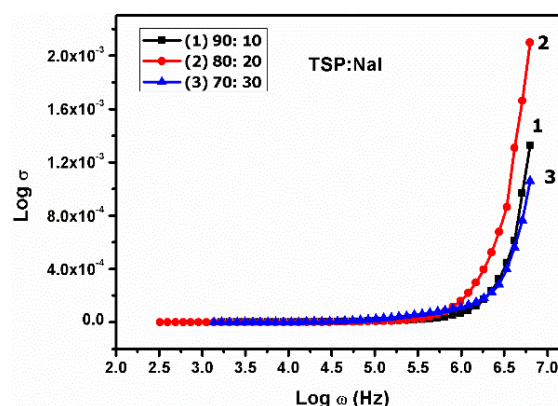
3.6. Behaviour of Conductance Spectra

Fig. 6 illustrates the frequency dependence of TSP and NaI composite electrolytes across three distinct compositional configurations. The results are represented on a logarithmic scale, plotting Log σ (AC conductivity) against Log ω (angular frequency) [14]. Such graphical representations are conventionally employed to analyse the conduction mechanisms inherent in solid-state electrolytes.

Within the low-frequency domain (Log ω≈ 2.0 to 5.5), the conductivity remains relatively invariant across all samples, establishing a plateau region. This segment marks the DC conductivity regime, in which long-range ionic transport is dominant. The plateau indicates a consistent flow of charge carriers, remaining unaffected by fluctuations in frequency. The composite of 80% TSP:20% NaI demonstrates the highest baseline conductivity, suggesting a more efficient mechanism for ionic transport compared to the 10% and 30% configurations.

As one moves beyond Log ω≈ 6.0, a pronounced increase in conductivity is observed across all compositional variants. This frequency-dependent escalation in σ is indicative of AC conductivity behaviour, wherein localised ionic hopping between sites becomes increasingly significant. The observed increase implies a transition from long-range to short-range dynamic ionic movement. Notably, the 80% TSP:20% NaI sample consistently maintains the highest conductivity across this frequency range, indicating enhanced ionic mobility and reduced energy barriers associated with ionic hopping.

Fig. 6. Conductance spectra plot for TSP-NaI at different wt.% ratios

The compositional makeup exerts a pivotal influence on the conductivity profile. The 80% TSP:20% NaI configuration surpasses the others across the entire frequency spectrum. In the 90% TSP:10% NaI system, the constrained salt content

likely limits the availability of free charge carriers, leading to reduced conductivity. Conversely, although the 70% TSP:30% NaI composition contains a higher proportion of NaI, its conductivity is marginally lower than that of the 80% sample, which may inhibit effective ionic mobility. The Log σ versus Log ω graph unequivocally shows that the 80% TSP:20% NaI composite exhibits superior conductivity among the compositions investigated.

3.7. Behaviour of Tangent Loss

The graph (Fig. 7) delineates the fluctuation of the dielectric loss tangent (tan δ) in relation to frequency (denoted as Log ω) for TSP:NaI composites exhibiting diverse compositions. The dielectric loss tangent (tan δ) serves as an indicator of energy dissipation within a dielectric substance and is quantitatively defined as the ratio of the imaginary component (ε^{11}) to the real component (ε^1) of the complex permittivity [15]

$$\text{Tan } \delta = \frac{\varepsilon^{11}}{\varepsilon^1} \tag{4}$$
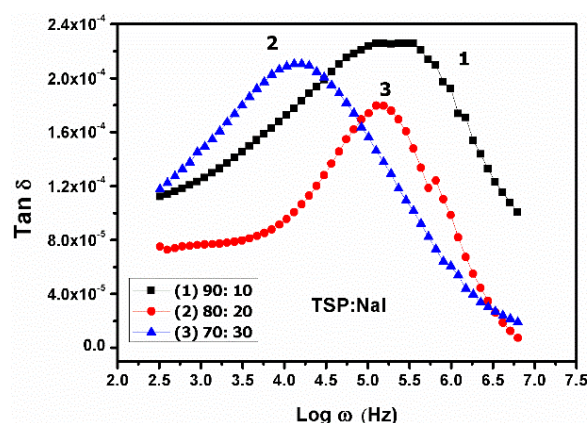

Fig. 7. Tangent loss spectra plot for TSP-NaI at different wt.% ratios

The graphical representation serves as a tool for evaluating relaxation phenomena and the efficacy of energy storage within composite materials subjected to an alternating electric field. Each formulation exhibits a unique apex in tan δ, indicating a dielectric relaxation mechanism in which the dipoles or mobile ions in the system synchronise with the externally applied field. The existence of such an apex substantiates the assertion that the system experiences a transition from long-range to localised ionic dynamics. The displacement of the peak's position with composition implies that the relaxation time (τ), which is inversely related to the frequency at which the peak is observed, is contingent upon the

composition.

$$\omega_{max} = \frac{1}{\tau} \tag{5}$$

The sample consisting of 80% TSP and 20% NaI exhibits the lowest peak value at a comparatively lower frequency, indicating an extended ion relaxation time. In contrast, the sample comprising 90% TSP and 10% NaI exhibits a peak at a higher frequency (indicating a reduced τ), implying a more accelerated dielectric relaxation. The variability of the magnitude of 'tan δ' is pronounced across the different compositions. The 90% TSP: 10% NaI configuration exhibits the most significant peak, indicating the highest level of dielectric loss, potentially attributable to an elevated ion concentration that promotes interfacial polarisation and energy dissipation. The 70% TSP: 30% NaI formulation reveals a moderate 'tan δ' peak, likely indicative of optimal conditions concerning ion mobility and matrix stability. Conversely, the 80% TSP:20% NaI formulation exhibits a more pronounced peak value of 2.12×10^{-4}, associated with expedited polarisation processes but diminished energy dissipation due to a lower density of mobile ions. The loss tangent values are delineated in Table 3.

3.8. Optical Absorption Bandgap

The derived empirical values are listed in Table 4. The optical absorption bandgap for pristine TSP, quantified at 3.92 eV, is observed to exhibit a gradual decline, ultimately reaching a minimum value of 2.68 eV for the film composition characterised by an 80% TSP to 20% NaI ratio (Fig. 8). As the concentration of salt escalates in the 80:20 ratio film, a notable increment in all recorded bandgap values is identified. The increase in salt infusion may reduce bandgap values, attributable to the emergence of new localised electron states within the band gaps of the host polymer matrix. These newly established states function as sites for trapping or recombination, thereby facilitating the transit of electrons from the valence band to these emergent bands and subsequently to the conduction bands [16].

The prior investigations have also indicated that the 80:20 ratio exhibits the highest degree of amorphous character and the lowest activation energy among the films synthesised. These findings lead us to infer that incorporating salt concentration promotes the development of an amorphous phase and establishes bonding interactions between the polymer chains and the salt, which consequently

diminishes the activation energy and induces a reduced energy bandgap up to the 80:20 ratio.
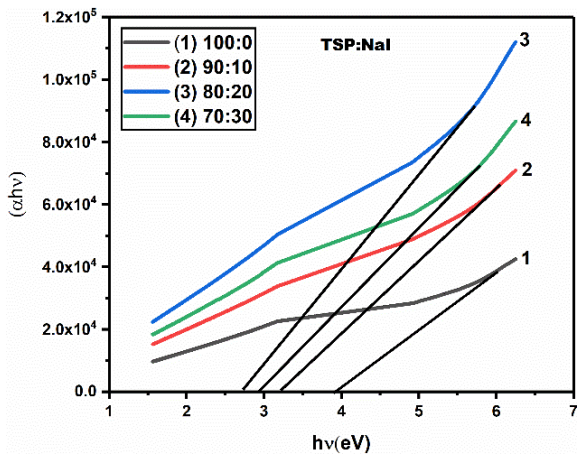

Fig. 8. Optical absorption bandgap plot for different wt.% ratios of TSP-NaI

3.9. Optical Energy Bandgap

The band structure of a given material can be determined by analysing optical absorption phenomena. The energy difference between the conduction and valence bands is called the bandgap. The energy level at which photons are absorbed is identified as the optical bandgap. Band gaps can be categorised into two distinct types based on the material properties: (i) Direct band gaps, characterised by uniformity between the valence and conduction bands, with zero crystal momentum; and (ii) Indirect band gaps, where there exists a disparity between the valence and conduction bands, accompanied by non-zero crystal momentum. Additionally, solid-state physics elucidates that solid materials exhibit energy spectra that encompass forbidden energy levels. This implies that in such systems, transition activity is confined to high-energy photons, consequently leading to the non-absorption of free charge carriers. Thus, although optical forbidden energy band gaps exist, certain band gaps are indeed allowed.

At elevated absorption coefficients, the formula proposed by Mott, Davis, and Tauc correlates the energy of incident photons with the absorption coefficient for amorphous materials.

$$\alpha h\nu = B\,(h\nu - E_g)^m \tag{6}$$

Where m represents an index, 'B' denotes a constant, and 'E_g' signifies the optical energy gap. The specific electronic transitions that contribute to the optical absorption depend on the value of m. For transitions categorised as direct-allowed, direct-forbidden, indirect-allowed, and indirect-forbidden, m can assume the values of 1/2, 3/2, 2, and 3, respectively. The optical absorption threshold, absorption transmission, and the migration of electrons from the valence band to the conduction band are all influenced by the wavelength or photon energy (hv) [17]. Tauc's plot of $(\alpha h\nu)^X$ against photon energy (hv) serves as a method for ascertaining the energy bandgap, wherein, based on the equation, x is defined as 1/m. Fig. 9 and 10 illustrate the results of the energy bandgap for the direct allowed electronic transition (x= 1/m= 2) and the direct forbidden electronic transition (x= 1/m =2/3), respectively. Fig. 11 and 12 depict the indirect allowed transition (x= 1/m= 1/2) and the indirect forbidden transition (x= 1/m= 1/3), respectively. From these graphical representations, the associated values of the optical energy bandgap are extracted and compiled in Table 4.
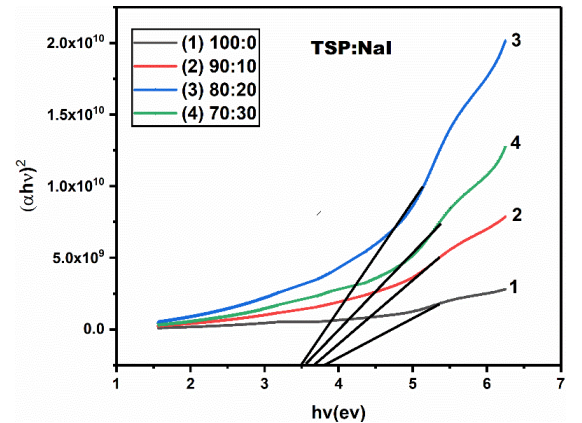

Fig. 9. 'Direct allowed energy bandgap' plot for different wt.% ratios of TSP-NaI

Table 4. Optical bandgap parameters for different wt.% ratios of TSP-NaI

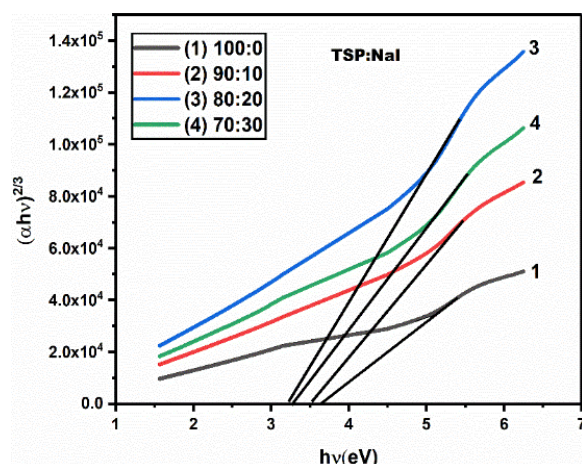| TSP:NaI compositions	Absorption band gap (eV) $(\alpha h\nu):h\nu$	Direct allowed band gap (eV) $(\alpha h\nu)^2:h\nu$	Direct forbidden band gap (eV) $(\alpha h\nu)^{2/3}:h\nu$	Indirect allowed band gap (eV) $(\alpha h\nu)^{1/2}:h\nu$	Indirect forbidden band gap (eV) $(\alpha h\nu)^{1/3}:h\nu$	Urbach Energy (eV)
100:00	3.92	3.81	3.64	3.08	2.96	4.22
90:10	3.19	3.68	3.51	2.65	2.55	3.92
80:20	2.68	3.42	3.19	2.21	2.29	3.42
70:30	2.93	3.61	3.26	2.45	2.33	3.65

Fig. 10. 'Direct forbidden energy bandgap' plot for different wt.% ratios of TSP-NaI
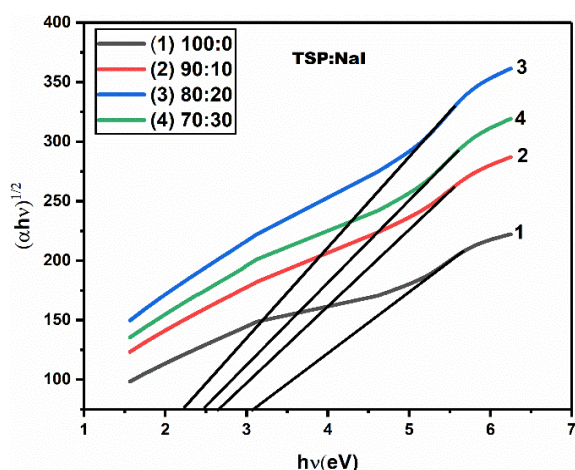

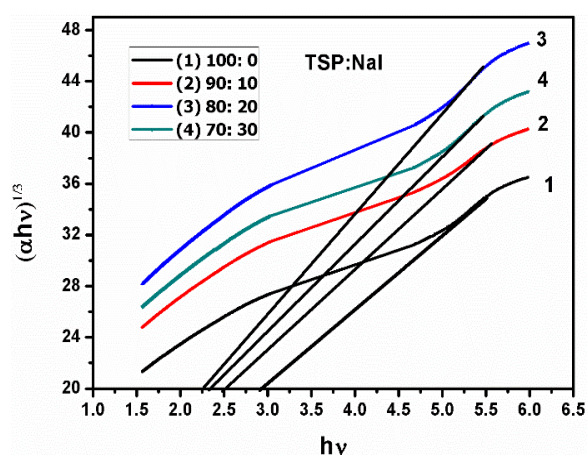**Fig. 11.** 'Indirect allowed bandgap' for different wt.% ratios of TSP-NaI

Fig. 12. 'Indirect forbidden bandgap' for different wt.% ratios of TSP-NaI

By obtaining the intercept of the constructed linear representations with the energy axis of the

plots [18], all bandgap values are ascertained. In all four optical energy bandgap categories for pure TSP, an initial high value is observed, which subsequently decreases to the lowest value for a film with an 80% TSP:20% NaI ratio. As the salt concentration is further elevated beyond the 80:20 ratio film, all bandgap values increase again. Variations in salt infusion may alter bandgap values by forming new localised electron states within the bandgaps of the host polymer matrix [19].

3.10. Urbach Energy

The Urbach empirical rule elucidates the extended tail observed in absorption spectra at low photon energies below the band edge. The Urbach energy quantifies the energy disorder present at the band edges, also referred to as the Urbach edge, and is characterised by energy dimensions. This quantity is ascertained by fitting the absorption coefficient as a function of energy to an exponential model. The relationship between absorption and energy is expressed by the following equation [20].

$$\alpha = \alpha_0 e^{\frac{(h\nu - E_g)}{E_U}} \qquad (7)$$

Where E_U denotes the Urbach energy and 'α_0' and 'E_g' represent fitting parameters with dimensions of inverse length and energy, respectively. This equation is valid solely under the condition that 'α' is directly proportional to exp ($h\nu$). The Urbach Energy exhibits variability due to temperature fluctuations. Figure 13 illustrates the relationship between energy '$h\nu$' and 'Ln(α)'. By analysing the slope of the resultant linear graphs in relation to the energy axis, the Urbach energy can be deduced from the graphical representation [21]. The slopes corresponding to various polymer electrolyte film compositions are depicted in the inset graphs.
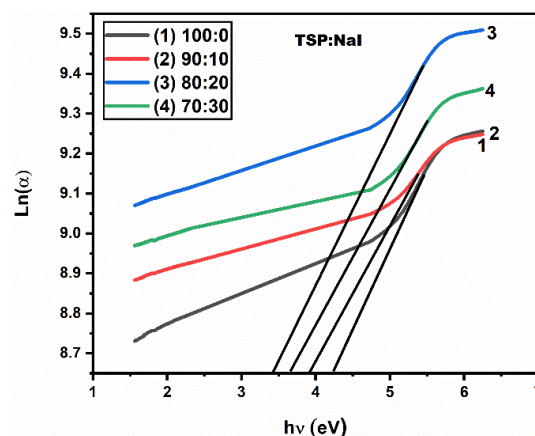

Fig. 13. 'Urbach energy' plot for different wt.% ratios of TSP-NaI

The band gaps derived from the Urbach energy assessments for multiple TSP-NaI compositions are presented in Table 4. The table indicates that the Urbach energy is influenced by an increase in salt concentration, attaining a peak at an 80:20 weight percent film composition. This trend corroborates the inverse correlation observed between band gap energy and Urbach energy. Abdullah et al. [22] documented analogous results.

3.11. Optical Dielectric Loss

Fig. 14 elucidates the variation of the imaginary component of the dielectric constant ($\varepsilon_i = 2 \mu k$), respectively, as a function of photon energy (hv) for TSP: NaI composites with varying ratios. Here, 'k denotes the extinction coefficient, and 'μ represents the refractive index.

An increase in NaI content correlates with a rise in ε_i, particularly for energy values exceeding 5.0 eV, indicating enhanced optical absorption due to increased electronic transitions. The pronounced increases around ~5.5–6.0 eV signify the commencement of interbond transitions. The 80:20 compositional ratios display the highest ε_i, suggesting optimal doping levels for enhanced optical activity [23]. These findings imply that incorporating NaI significantly enhances the material's polarizability and absorption. The low-energy spectrum (~1.0–4.5 eV) reveals minimal variation, indicating that absorption is predominantly influenced within the higher-energy ultraviolet range. This tunability of ε_i via NaI doping could be advantageous for optoelectronic applications [24]. A slight reduction in ε_i relative to the 80:20 composition may be attributed to structural disorder. This behaviour indicates the presence of a critical concentration necessary for optimal optical performance.
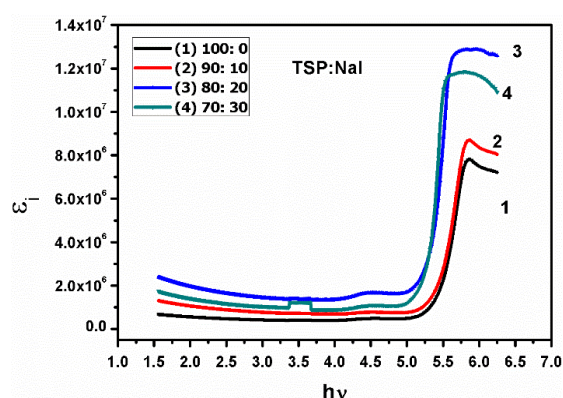
The graph (Fig. 15) presented above illustrates the variations of the fundamental component of the optical dielectric constant ($\varepsilon_r = \mu^2 - k^2$) as a function of photon energy (hv) for TSP:NaI biopolymer electrolyte films with diverse compositions (100:0, 90:10, 80:20, and 70:30 wt.%). The dielectric constant indicates a material's ability to store electrical energy and is strongly influenced by its electronic architecture and degree of polarizability [25]. Upon review of the graph, it is evident that all compositions exhibit a steady decline in ε_r with increasing photon energy, culminating in a sharp drop in the range 5.5-6.0 eV. This decline marks the onset of substantial optical absorption due to interband electronic transitions, in which electrons migrate from the valence band to the conduction band. Among the various compositions, the 80:20 TSP:NaI film (Fig. 15) displays the most notable variation, suggesting increased optical activity along with more significant electronic polarisation effects. The observed reduction in ε_r with increasing energy indicates that at higher photon energies, the dipoles within the material cannot synchronise with the rapidly oscillating optical field, ultimately resulting in reduced polarisation. The significant dielectric response of the 80:20 composition corresponds to its minimal optical band gap (2.68 eV) and maximal Urbach energy, both of which indicate an increase in structural disorder and enhanced electronic transitions. As a result, the graph corroborates that the 80:20 TSP-NaI formulation demonstrates enhanced optical dielectric characteristics, integrating elevated low-energy polarizability with efficient electronic excitation.
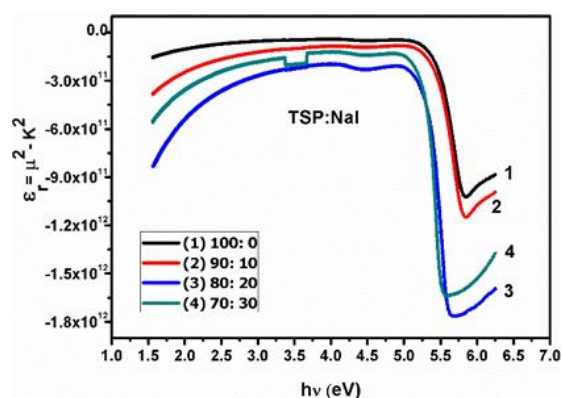

Fig. 15. 'Real part of optical dielectric loss' for different wt.% ratios of TSP-NaI

4. CONCLUSIONS

The synthesis of biopolymer electrolyte films was

Fig. 14. Imaginary part of optical dielectric loss for different wt.% ratios of TSP-NaI

accomplished using the solution-casting technique, incorporating Tamarind Seed Polysaccharide (TSP) with various concentrations of Sodium Iodide (NaI). The 80:20 weight ratio yielded a homogeneous, pliable film. XRD analysis indicated that this composition exhibited the highest degree of amorphousness and the smallest crystallite dimensions (0.31 nm), which markedly enhances ionic conduction. FTIR spectroscopy confirmed the formation of a complex between TSP and NaI, as evidenced by shifts in functional group bands attributable to salt-polymer interactions. Measurements of temperature dependence of conductivity indicated that the 80:20 composition possessed the highest ionic conductivity (1.97×10^{-4} S/cm) alongside the lowest activation energy (0.69 eV), consistent with Arrhenius-type behaviour. Dielectric investigations revealed a peak in dielectric permittivity and dielectric loss at lower frequencies, indicating enhanced space-charge polarisation and increased ion mobility. The analysis of tangent loss corroborated these results, demonstrating an optimal relaxation profile for the 80% TSP:20% NaI composition. Optical absorption analyses revealed a reduction in the bandgap from 3.92 eV (pure TSP) to 2.68 eV, suggesting improved electronic transitions due to localised states. The examination of the optical bandgap confirmed lower-energy transitions in the 80:20 film, thereby endorsing its efficient conduction and absorption properties. Ultimately, the Urbach energy exhibited the highest value for the 80:20 film, indicating greater structural disorder, which is conducive to enhanced conductivity and optical responsiveness.

ACKNOWLEDGEMENT

REFERENCES

[1] Chattopadhyay, J., Pathak, T. S. and Santos, D. M. F., "Applications of polymer electrolytes in lithium-ion batteries: a review", Polymers, 2023. 15(19), 3907.

[2] Long, L., Wang, S., Xiao, M. and Meng, Y., "Polymer electrolytes for lithium polymer batteries", J. Mater. Chem. A, 2016. 4(26), 10038–10069.

[3] Saha, A., Kumar, K. V., Jyothi, N. K., Kiran, M. G. and Rao, M. C., "Structural and electrical properties of TSP: CH_2COONa amorphous biopolymer electrolytes for electrochemical cell applications", J. Non-Cryst. Solids, 2023. 616, 122465.

[4] Zhang, H., Cui, H., Xie, F., Song, Z. and Ai, L., "Tamarind seeds polysaccharide: Structure, properties, health benefits, modification and food applications", Food Hydrocoll., 2024. 110222.

[5] Cyriac, V., Noor, I. M. I., Mishra, K., Chavan, C., Bhajantri, R. F. and Masti, S. P., "Ionic conductivity enhancement of PVA: carboxymethyl cellulose poly-blend electrolyte films through the doping of NaI salt", Cellulose, 2022. 29(6), 3271–3291.

[6] Sampathkumar, L., Christopher Selvin, P., Selvasekarapandian, S., Perumal, P., Chitra, R., Muthukrishnan, M., "Synthesis and characterization of biopolymer electrolyte based on tamarind seed polysaccharide, lithium perchlorate and ethylene carbonate for electrochemical applications", Ionics (Kiel), 2019, 25 (3), 1067–1082.

[7] Nandini PS., Madala S., Basamma S., Satyanarayana JV., Ch S., Keerthi M., Rao MC., "Structural and Thermal Studies of $NaNO_3$-based Polymer Electrolytes for Battery Applications", ECS Journal of Solid State Science and Technology, 2025, 7,14(5),053003.

[8] Payandeh S, remhof A., battaglia C., "Solid-state Magnesium-ion Magnesium Batteries" Research and Applications, 2019, 23, 60.

[9] Yong, J., Shamsuri, N. A., Bashir, A. B., Kadir, M. F. Z. and Shukur, M. F. A., "Effect of ammonium thiocyanate (NH_3SCN) concentration on the ionic transport in dextran-based polymer electrolyte", Mol. Cryst. Liq. Cryst., 2023. 764(1), 55–69.

[10] Pandey, A., Dalal, S., Dutta, S. and Dixit, A., "Structural characterization of poly-crystalline thin films by X-ray diffraction

techniques", J. Mater. Sci. Mater. Electron., 2021. 32, 1341–1368.

[11] Nandiyanto, A. B. D., Ragadhita, R. and Fiandini, M., "Interpretation of Fourier transform infrared spectra (FTIR): A practical approach in the polymer/plastic thermal decomposition", Indones. J. Sci. Technol., 2023. 8(1), 113–126.

[12] Chandra, A., Chandra, A., Dhundhel, R. S. and Bhatt, A., "Sodium-ion-conducting solid polymer electrolyte: temperature-dependent ionic parameters and solid-state polymer battery fabrication", Indian J. Phys., 2022. 96(4), 1069–1074.

[13] Szafrański, M., "Phase transitions studied by high-pressure dielectric spectroscopy and calorimetry in High-pressure Crystallography", Springer Netherlands, Dordrecht, 2004. 295–310.

[14] Bonneau, H., Avni, Y., Andelman, D. and Orland, H., "Frequency-dependent conductivity of concentrated electrolytes: A stochastic density functional theory", J. Chem. Phys., 2024. 161(24).

[15] Yablon, D. G., Grabowski, J. and Chakraborty, I., "Measuring the loss tangent of polymer materials with atomic force microscopy-based methods", Meas. Sci. Technol., 2014. 25(5), 055402.

[16] Haque, B. M., Chandra, D. B., Jiban, P., Nurul, I. and Abdullah, Z. J. M. S. i. S. P., "Influence of Fe^{2+}/Fe^{3+} ions in tuning the optical band gap of SnO_2 nanoparticles synthesized by TSP method: surface morphology, structural and optical studies", Mater. Sci. Semicond. Process, 2019. 89, 223–233.

[17] Alsulaim, G. M. and Elamin, A. A., "Two promising methodologies for dealing with changes in optical and electrical properties of polymer electrolytes (SPEs)", J. Compos. Sci., 2023. 7(6), 221.

[18] Aziz, S. B., Abdullah, O. G., Hussein, A. M., Abdulwahid, R. T., Rasheed, M. A., Ahmed, H. M., Abdalqadir, S. W. and Mohammed, A. R., "Optical properties of pure and doped PVA: PEO based solid polymer blend electrolytes: two methods for band gap study", J. Mater. Sci. Mater. Electron., 2017. 28, 7473–7479.

[19] Ahmad, H. M., Sabeeh, S. H. and Hussein, S. A., "Electrical and optical properties of PVA/LiI polymer electrolyte films", Asian Trans. Sci. Technol., 2012. 1(6), 16–20.

[20] Aziz, S. B., Abdullah, O. G., Hussein, A. M., Abdulwahid, R. T., Rasheed, M. A., Ahmed, H. M., Abdalqadir, S. W. and Mohammed, A. R., "Optical properties of pure and doped PVA: PEO based solid polymer blend electrolytes: two methods for band gap study", J. Mater. Sci.: Mater. Electron., 2017. 28, 7473–7479.

[21] Muhammad, F. F., Aziz, S. B. and Hussein, S. A., "Effect of the dopant salt on the optical parameters of PVA: $NaNO_3$ solid polymer electrolyte", J. Mater. Sci. Mater. Electron., 2015. 26, 521–529.

[22] Hussein, A. M., Dannoun, E. M. A., Aziz, S. B., Brza, M. A., Abdulwahid, R. T., Hussen, S. A., Rostam, S., Mustafa, D. M. T. and Muhammad, D. S., "Steps toward the band gap identification in polystyrene-based solid polymer nanocomposites integrated with tin titanate nanoparticles", Polymers, 2020. 12(10), 2320.

[23] Aziz, S. B., Brza, M. A., Nofal, M. M., Abdulwahid, R. T., Hussen, S. A., Hussein, A. M. and Karim, W. O., "A comprehensive review on optical properties of polymer electrolytes and composites", Materials, 2020. 13(17), 3675.

[24] Heiba, Z. K., El-Naggar, A. M., Kamal, A. M., Abd-Elkader, O. H. and Mohamed, M. B., "Optical and dielectric properties of $PVC/TiO_2/TBAI$ ionic liquid polymer electrolyte", Opt. Mater., 2023. 139, 113764.

[25] Abarna, S. and Hirankumar, G., "Vibrational, electrical, dielectric and optical properties of PVA-LiPF6 solid polymer electrolytes", Mater. Sci.-Pol., 2019. 37(3), 331–337.

131